Stationary and Non-stationary Temperature-Duration-Frequency Curves for Australia

Orpita U Laz
Western Sydney University
Ataur Rahman (a.rahman@westernsydney.edu.au)
Western Sydney University
Taha B M J Ouarda
Institut national de la recherche scientifique INRS-ETE
Nasreen Jahan
Bangladesh University of Engineering and Technology

Research Article

Keywords: Annual maximum temperature, Climate change, Climate drivers, Generalised Extreme Value, Non-stationary, Temperature-Duration-Frequency

Posted Date: April 6th, 2023

DOI: https://doi.org/10.21203/rs.3.rs-2778999/v1

Additional Declarations: No competing interests reported.

Stationary and Non-stationary Temperature-Duration-Frequency Curves for Australia

Orpita U Laz,[a] Ataur Rahman,[a,*] Taha B M J Ouarda,[b] Nasreen Jahan [c]

[a] *School of Engineering, Design and Built Environment, Western Sydney University, Locked Bag 1797, Penrith NSW 2751, Australia.*

[b] *Canada Research Chair in Statistical Hydro-Climatology, Institut national de la recherche scientifique INRS-ETE, Quebec, Canada*

[c] *Professor, Department of Water Resources Engineering, Bangladesh University of Engineering and Technology, Bangladesh, email: nasreenjahan@wre.buet.ac.bd*

*Corresponding author: a.rahman@westernsydney.edu.au

Acknowledgments.

The authors would like to acknowledge the Australian Bureau of Meteorology and National Oceanic and Atmospheric Administration for providing data. The authors declare that no funding was received for this study. The authors also declare that there is no conflict of interest to declare.

ABSTRACT

Australian summer heat events have become more frequent and severe in recent times. Temperature-duration-frequency (TDF) curves connect the severity of heat episodes of various durations to their frequencies and thus can be an effective tool for analysing the heat extremes. This study examines Australian heat events using data from 82 meteorological stations. TDF curves have been developed under stationary and non-stationary conditions. Generalised Extreme Value (GEV) distribution is considered to estimate extreme temperatures for return periods of 2, 5, 10, 25, 50 and 100 years. Three major climate drivers for Australia have been considered as potential covariates along with *Time* to develop the non-stationary TDF curves. According to the Akaike information criterion, the non-stationary framework for TDF modelling provides a better fit to the data than its stationary equivalent. The findings can be beneficial in offering new information to aid climate adaptation and mitigation at the regional level in Australia.

Keywords: Annual maximum temperature; Climate change; Climate drivers; Generalised Extreme Value; Non-stationary; Temperature-Duration-Frequency.

1. INTRODUCTION

Intergovernmental Panel on Climate Change (IPCC) estimated that the mean global temperature would exceed the higher limit of increase in temperature adopted in the Paris agreement by the 2040s (IPCC, 2018). It was also reported in 2020 that the temperature in Australia has increased by 1.44 ± 0.24 °C since 1910 (CSIRO and Australian Government (Bureau of Meteorology), 2020). Generally, changes in maximum and minimum temperatures impact the environment more than mean temperature (Sein, Chidthaisong and Oo, 2018) and adversely influence the events related to extreme temperature (Chowdary, John and Gnanaseelan, 2014). Extreme temperature triggers more natural hazards, i.e. droughts, bushfires, heatwaves, cyclones, and negatively affects human health, agriculture, ecosystems and infrastructure (Omer *et al.*, 2020; Suman and Maity, 2020). Therefore, predicting extreme temperatures for a particular duration and return period is important in many aspects of our lives. Some are relevant to health, energy and agriculture, urban planning, and ecology management. In this context, the design temperatures for the selected durations and return periods can be estimated following the same principle of rainfall Intensity-Duration-Frequency (IDF) curves, which have been utilised for many years for the design and management of hydrological infrastructure as well as flood risk management (Yan *et al.*, 2019). Extreme value theory has been accepted globally to construct IDF curves by fitting theoretical probability distribution functions to annual maximum rainfall time series (Cheng and Aghakouchak, 2014; Yan *et al.*, 2020).

Most of the works found in the literature on IDF curves are based on the temporal stationary concept (Singh and Zhang, 2007; Jakob, 2013), implying that the occurrence probability of precipitation events will not change significantly over time. However, in reality, the frequency, magnitude and duration of hydroclimatic extremes, i.e. extreme rainfall (Galiatsatou and Iliadis, 2022), floods (Berghuijs *et al.*, 2019), droughts (Spinoni, Naumann and Vogt, 2017), and heatwaves (Lorenz, Stalhandske and Fischer, 2019) fluctuates beyond the stationary envelope of variability. Furthermore, it is also observed that the IDF curve considering stationarity, often underestimates the return level of rainfall (Sugahara, da Rocha and Silveira, 2009; Cheng and Aghakouchak, 2014). Therefore, to increase the reliability of IDF curves, it is suggested to incorporate the non-stationarity of the distribution parameters in hydrological models (Sarhadi and Soulis, 2017), especially at their extreme levels (Ganguli and Coulibaly, 2017).

In the construction of IDF curves, covariates are generally introduced to apprehend the non-stationarities in time series. Any drivers that are correlated to the selected events can be considered as a candidate for such covariates (Katz, Parlange and Naveau, 2002; Hundecha *et al.*, 2008), which can be low-frequency climatological signals (Coles, 2001) as well as time (Sugahara, da Rocha and Silveira, 2009; Yilmaz and Perera, 2014). In this approach, the parameters of the Generalised Extreme Value

(GEV) distribution are expressed as a linear or non-linear function of covariates (Kwon and Lall, 2016; Sarhadi and Soulis, 2017). This approach has been effectively employed in extreme rainfall events around the world (Ouarda, Yousef and Charron, 2019), including in Australia (Yilmaz and Perera, 2014).

Although there have been extensive works carried out on the development of IDF curves all over the globe, very limited works are found in the literature on the construction of Temperature-Duration-Frequency (TDF) curves, which relate temperature intensities corresponding to varying durations and return periods (Wang *et al.*, 2013; Ouarda and Charron, 2018a). Moreover, no TDF curves have been constructed for Australia till date.

In this study, time series data of the daily maximum temperature of Australia at selected stations are analysed, and the best climate-informed covariates are selected from the most influential covariates for the annual maximum temperature to characterise the physical process related to the dynamics of the extreme temperature. For this purpose, three climate drivers, namely – El Niño Southern Oscillation (ENSO), Southern Annular Mode (SAM) and Indian Ocean Dipole (IOD), are selected along with the *Time* as potential covariates. After that, stationary TDF curves are constructed following the frequency analysis method, already adopted in the construction of IDF curves, for different durations and return periods. The present work also extends these stationary TDF curves to non-stationary conditions according to the framework outlined by Ouarda and Charron (2018b). Then, based on the Akaike Information Criterion (AIC) value, the best model for each selected station is identified, and the TDF curves are constructed under stationary and non-stationary conditions. Finally, the influence of non-stationarity on the TDF curves is assessed.

2. STUDY AREA AND DATA

The whole Australia is considered as the study area except Tasmania (Figure 1). Australia experiences a variety of climates across the country because of a wide range of geographical extent consisting of tropical-influenced climate in the northern and north-eastern zones, Mediterranean-like climate in the southern coastal zones and desert climate in most of the central interior zones (Turney *et al.*, 2007).

2.1 Temperature time series

All the recorded daily maximum temperatures across Australia weather stations were examined for inconsistency, outliers and gaps. The stations, which had less than 5% missing data over the last five decades covering the time period from 1969 to 2021, were selected for analysis. According to the abovementioned criterion, 82 weather stations in Australia (out of 1415 weather stations) were selected.

The gaps in the daily maximum temperature time series in the selected stations were spatially interpolated with the same time series data from surrounding weather stations located within a 30 km radius. The locations of the selected temperature stations are shown in Figure 1.

The annual maximum daily temperatures were calculated for each selected weather station from the recorded daily maximum temperature data. Particular attention was given to the summer season of Australia, which is considered to be December to February, and the extended summer is considered to be from November to March. Therefore, the annual maximum daily temperature calculated from each calendar year would have been divided into summer or extended summer seasons into two consecutive years. Therefore, the hydrologic year in Australia, starting from April to March, instead of the calendar year, was considered in this study to calculate the annual maximum daily temperature.

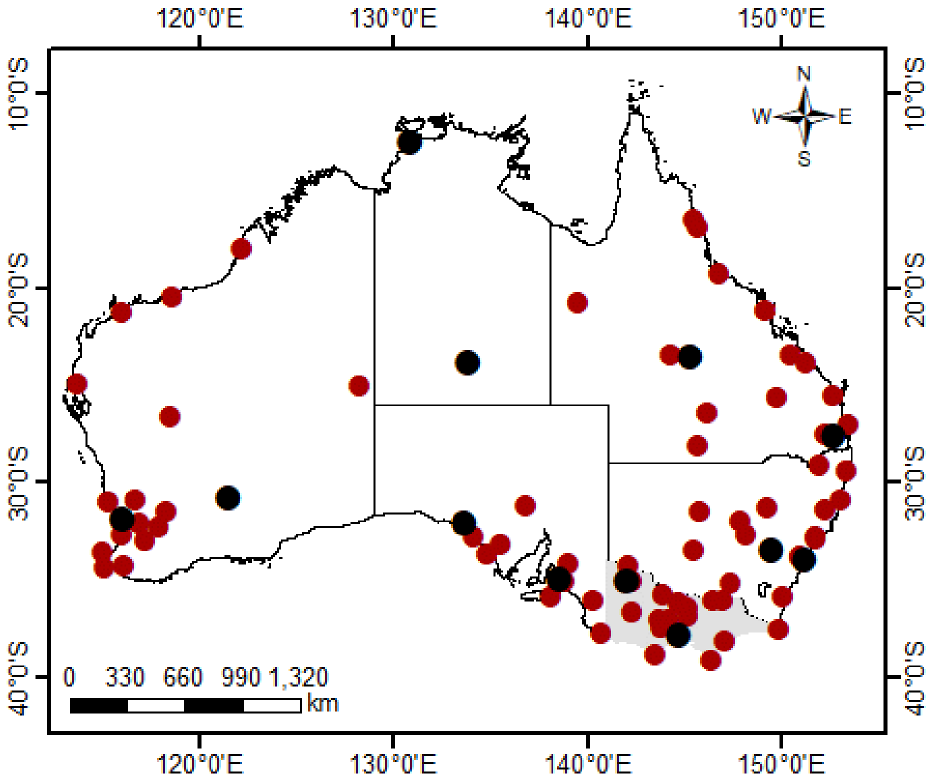

Figure 1. Study area and selected stations (stations marked with black circles are described in detail in this paper).

2.2 Covariates

Australia is extremely susceptible to changes in the ocean-atmosphere system. The inter-annual dynamics of Australia's seasonal weather are regulated by the climatic variability of three neighbouring oceans – the Pacific, Indian, and Southern Oceans (Cai *et al.*, 2014; Maher and Sherwood, 2014;

Oliveira and Ambrizzi, 2017), known as climate drivers. Three primary climate drivers strongly influence Hydroclimate in Australia – The El Niño Southern Oscillation (ENSO) (Power *et al.*, 1999; Cai and Van Rensch, 2012), Southern Annular Mode (SAM) (Thompson, Wallace and Hegerl, 2000; Risbey *et al.*, 2009) and Indian Ocean Dipole (IOD) (Ummenhofer *et al.*, 2009, 2011).

Therefore, in this study, three physical processes, in which two of them from the sea surface temperature – ENSO, IOD and one from air pressure – SAM, and also *Time,* were considered to be one of the potential covariates to identify the best covariate for developing non-stationarity TDF curves.

i. El Niño-Southern Oscillation (ENSO) cycle

The El Nino-Southern Oscillation (ENSO) is considered to be a major climate driver over many regions of the globe (Ropelewski and Halpert, 1988; Halpert and Ropelewski, 1992), including Australia (Nicholls, 1985). The SST index is considered the monthly sea surface temperature anomaly over NINO 3.4 (17 °E–120 °W, 5 °S–5 °N) region (Bellenger *et al.*, 2014) and was used as a covariate representing ENSO. Nino3.4 was obtained from https://psl.noaa.gov/gcos_wgsp/Timeseries/Nino34.

ENSO is considered to be a strong climate driver in Australia (Power *et al.*, 2006; Risbey *et al.*, 2009; Arblaster and Alexander, 2012), especially in southeastern Australia (Nicholls and Lucas, 2007) and northeast Australia (Min, Cai and Whetton, 2013; Cowan *et al.*, 2014; Perkins, Argüeso and White, 2015), but weak in the far southeast of Australia (Parker, Berry and Reeder, 2013; Boschat *et al.*, 2015). In Australia, it has been observed that the strength of ENSO decreases along a north-south gradient.

ii. Indian Ocean Dipole (IOD)

The Indian Ocean Dipole (IOD) is represented with Dipole Mode Index (DMI) (Saji *et al.*, 1999; Meyers *et al.*, 2007; Liu *et al.*, 2014) and calculated as the difference of SST anomalies in the western equatorial Indian Ocean (50 to 70°E, 10°S to 10°N) minus those in the east (90 to 110°E, 10°S to 0°). The monthly DMI was derived from https://psl.noaa.gov/gcos_wgsp/Timeseries/DMI/ and considered as a covariate that represents IOD.

IOD has been identified as the major driver for Eastern Australia (Meyers *et al.*, 2007; Risbey *et al.*, 2009; Cai *et al.*, 2011) and has a positive correlation with maximum temperatures during winter and spring (May and November) (Min, Cai and Whetton, 2013; White *et al.*, 2013).

iii. SAM

The Southern Annular Mode (SAM) describes the north-south movement of the westerly wind belt that circles Antarctica and is a monthly mean sea level pressure (MSLP) anomaly time dataset. The data for this index were obtained from http://www.nerc-bas.ac.uk/icd/gjma/sam.html.

SAM considerably impacts the rainfall in Australia (Hendon, Thompson and Wheeler, 2007), particularly in southern Australia. SAM is even associated with 10-15% of the rainfall in southwest Australia. SAM also affects the temperature in Australia and is identified as the main climate driver for the southwestern land division in western Australia (Guthrie, 2021).

iv. Time

Time has been utilised as a covariate to investigate the non-stationarity in the IDF curves all over the world (Sugahara, da Rocha and Silveira, 2009; Yilmaz and Perera, 2014). Therefore, in this study, *Time* was also considered as one of the potential covariates to construct the non-stationary TDF curves. The hydrological years of the annual maximum temperature series were transformed into a series of integers from 1 to the number of years of the selected time duration and considered as a covariate representing *Time*.

3. METHODOLOGY

In this study, firstly, the non-stationarity of the temperature data series was assessed to justify the requirements of the incorporation of the non-stationarity in the construction of TDF curves. Then, the correlations between the selected three physical processes - ENSO, SAM and IOD were computed to identify the best covariate. In this approach, *Time* was also used as one of the covariates. Different non-stationary models were constructed considering different covariates stated earlier as well as their combination. Finally, *time* or any of the selected physical processes (ENSO, IOD and SAM) was considered a covariate in Models with one covariate.

Similarly, *Time* and one climate index (*Time* – ENSO, *Time* – IOD and *Time* – SAM) were adopted in models with two covariates. First, the best model for the annual maximum temperature series was chosen based on the Akaike information criterion (AIC). After identifying the best non-stationary model, the non-stationary design temperature was computed using the parameters of the best non-stationary model.

GEV distribution was selected to develop both stationary and non-stationary TDF curves as it is widely used to develop model climatic extremes (Ouarda and Charron, 2018a; Ouarda, Charron and St-Hilaire, 2020; Haddad, 2021; Devi, Gouda and Lenka, 2022). Under the condition of stationary, three parameters of the GEV distributions, μ, σ, ξ, which are the location, scale and shape parameters, respectively, were assumed to be constant, whereas, under non-stationary conditions, the parameters were expressed as a linear or quadratic function of the covariate(s). However, the shape parameter was assumed to be constant for all the cases since the reliability of modelling the shape parameter is low (Cheng *et al.*, 2014; Ganguli and Coulibaly, 2017). The distribution parameters were calculated using the maximum composite likelihood method utilising the optimisation function *fmincon* in MATLAB. Finally, the stationary and non-stationary TDF curves were compared to assess the influence of non-stationarity in the construction of TDF curves.

3.1 Detection of non-stationarity in Temperature time series

All the historical records of annual maximum temperature at the selected stations over the selected time period were tested for non-stationary signals. An augmented Dickey-Fuller (ADF) test was applied to the annual maximum temperature data series for each of the selected stations. In this test, the null hypothesis assumes that the data series is non-stationary and thereby considered stationary when the null hypothesis is rejected at the selected significance level.

3.2 Correlation between climate drivers and temperature time series

The relations between the maximum annual temperatures for all the selected stations and climate drivers – ENSO, SAM and IOD were tested using correlation analyses considering both concurrent and time-lagged relationships.

The covariates representing climate drivers in this study were computed as the moving averages of corresponding climate drivers over three consecutive months starting from April and ending in March of the next year, covering the full hydrological year and denoted in this study by the first letter of the three months (AMJ, MJJ, JJA, JAS, ASO, SON, OND, NDJ, DJF, JFM). To determine the appropriate season of the climate driver acting as the predictor of the annual maximum temperature, correlations between seasonal climate drivers and annual maximum temperatures were explored. Best covariates and the suitable season were selected based on the higher correlation values between the annual maximum temperature series and climate drivers averaged over the selected season. This selection process was also validated graphically by plotting all the correlations between the annual maximum temperature time series and all the climate drivers for all seasons.

3.3 Construction of TDF curves

i. General TDF relationship

The general TDF relationship can be expressed by following the formulation for IDF curves proposed by (Rossi and Villani, 1994; Koutsoyiannis, Kozonis and Manetas, 1998):

$$t_R(d) = \frac{a(R)}{b(d)} \quad (1)$$

where, *d* is the duration and *R* is the return period. In this formulation, the dependency of return level, $t_R(d)$ on *R* and *d* can be modelled separately. The distribution of maximum average temperature *T(d)* governs the function *a(R)* that defines the TDF curves, which remain parallel for various return periods. The function *b(d)* controls the shape of the TDF curves and is given as:

$$b(d) = (d + \theta)^{\eta} \quad (2)$$

where, θ and η are the shape parameters subjected to the boundary conditions of $\theta > 0$ and $0 < \eta < 1$.

If the probability distribution of $T(d)$ is $F_{T(d)}(i; d)$, it will also be the distribution of $Y = T(d)b(d)$, which is the maximum average temperature scaled by $b(d)$ (i.e., $F_{T(d)}(i; d) = F_Y(y_T) = 1 - \frac{1}{T}$). Consequently, the expression $a(R)$ is given by:

$$a(R) = F_y^{-1}\left(1 - \frac{1}{R}\right) \quad (3)$$

ii. Stationary TDF curves

The GEV distribution is the most widely used probability distribution that is used to model climate extremes, and hence, the GEV distribution is used here to model *T(d)*. The cumulative distribution function of the GEV is given by:

$$F(x) = \exp\left\{-\left[1 + \kappa\left(\frac{x - \mu}{\sigma}\right)\right]^{-1/k}\right\}, \quad (4)$$

where, $\mu, \sigma\ and\ \kappa$ are the location, scale, and shape parameters, respectively. $F(x)$ is defined for $1 + \frac{\kappa(x - \mu)}{\sigma} > 0$, where $\sigma > 0$.

The general stationary TDF relationship based on the GEV distribution can be expressed as (Ouarda and Charron, 2018b):

$$t_R(d) = \frac{a\,(R)}{b(d)} = \frac{\mu - \frac{\sigma}{\kappa}\left\{1 - \left[\log\left(1 - \frac{1}{R}\right)^{-\kappa}\right]\right\}}{(d + \theta)^{\eta}} \tag{5}$$

iii. Non-stationary TDF curves

To incorporate non-stationarity in Equation (5), the three parameters of the GEV distribution described in Equation (4) are considered to be dependent on time to incorporate the non-stationarity in TDF curve development and Equation (4) can be expressed as:

$$F(x) = \exp\left\{- \left[1 + \kappa(t)\left(\frac{x - \mu(t)}{\sigma(t)}\right)\right]^{-1/k}\right\}, 1 + \frac{\kappa(t)(x - \mu(t))}{\sigma(t)} > 0 \tag{6}$$

In this study, the location and scale parameters are considered to vary with covariates linearly or quadratically, while all other shape parameters, θ, η and κ for the GEV distribution are assumed to be constant (Katz, Parlange and Naveau, 2002; Adlouni and Ouarda, 2009).

The vectors of the distribution parameters $\psi = (\mu, \sigma, \theta, \eta)$ and $\psi = (\mu_0, \mu_1, \ldots, \sigma_0, \sigma_1, \ldots, \kappa, \theta, \eta)$ are estimated using the maximum composite likelihood for stationary and non-stationary TDF curves, respectively.

4. RESULTS AND DISCUSSION

The results for 12 stations (two stations from each state in Australia and shown as black dots in Figure 1) are presented in greater detail (out of the 82 selected stations) in the following sections.

4.1 Detection of non-stationarity

The augmented Dickey-Fuller (ADF) test was applied to each annual maximum temperature data series separately for each selected station. Based on the ADF tests, the test statistics and p-value for 12 stations are summarised in Table 1. Four stations showed ADF test statistics below the critical value (-3.507), and the p-values were less than 0.05 at the 95% confidence level, as shown in boldface in Table 1. For these stations, the null hypothesis was rejected, and the data series was considered stationary. Therefore, the null hypothesis could not be rejected for the rest of the stations, and the non-stationarities in the data series were detected. Although all the available stationarity tests have some drawbacks and are not decisive alone (Cai, Cowan and Sullivan, 2009), the results of ADF tests here highlighted the presence of the non-stationarity in the temperature time series and consequently emphasised the importance of incorporating the non-stationarity in the construction of TDF curves.

Table 1. Summary of ADF test statistics and p-values for selected 12 stations in Australia.

Station ID	Station	p-value	Test statistics
066037	Sydney Airport AMO	0.465	-2.252
063005	Bathurst Agricultural Station	0.088	-3.246
014015	Darwin Airport	0.052	-3.493
015590	**Alice Springs Airport**	**0.008**	**-4.244**
009021	**Perth Airport**	**0.004**	**-4.579**
012038	Kalgoorlie-Boulder Airport	0.050	-3.506
040004	**Amberley AMO**	**0.006**	**-4.364**
036007	**Barcaldine Post Office**	**0.047**	**-3.532**
018012	Ceduna AMO	0.454	-2.275
023034	Adelaide Airport	0.060	-3.424
087031	Laverton RAAF	0.194	-2.829
076064	Walpeup Research	0.121	-3.088

4.2 Correlation analysis and covariate selection

The correlations between the annual maximum temperatures and the ENSO, IOD and SAM for all the seasons are presented spatially in Figures 2, 3 and 4, respectively.

The correlations between ENSO and the annual maximum temperatures were the strongest and statistically significant during the spring and summer seasons, particularly in the eastern regions of Australia. The positive influence of the ENSO on the temperature was weaker at the beginning of the hydrologic year and increased gradually over the year. At the end of the hydrological year, this influence became weak, even negative for some stations.

Similar to the ENSO, positive influences of IOD on the temperatures were also identified all over Australia. This influence was enhanced during the spring season and was statistically significant in the southeastern region of Australia. However, at the end of the hydrological year, the impact of IOD also became weaker and negative at some stations.

Unlike the other two climate drivers, SAM showed different relationships with the temperature in Australia. SAM exhibited a statistically significant positive relationship with the temperature at inland of the southeastern part during Autumn and negative relations with the temperature observed during spring at the stations in the western regions of Australia.

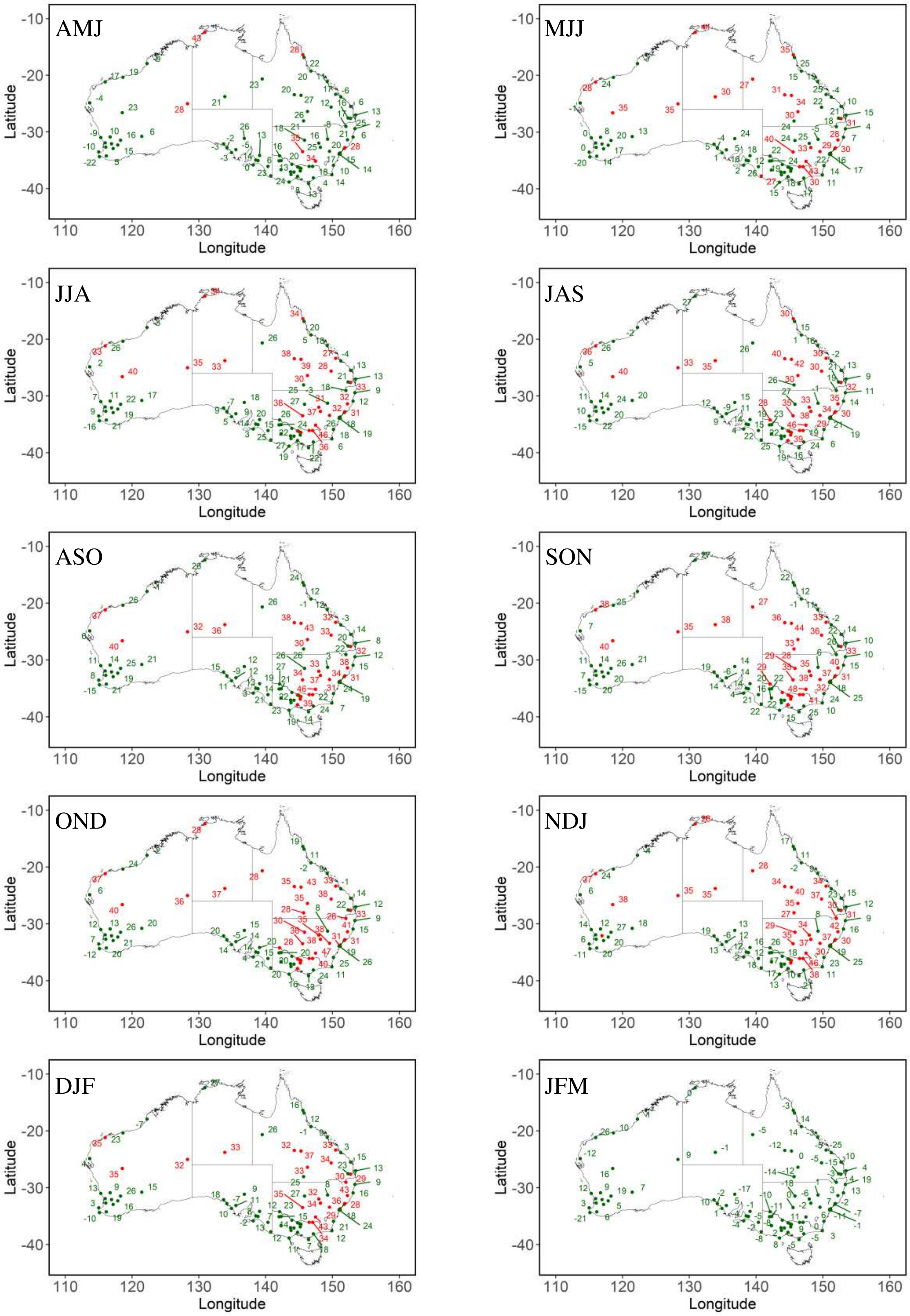

Figure 2. Spatial correlation of annual maximum temperature with ENSO during 1969 – 2021. Correlation values are multiplied by 100, and red values are statistically significant at a 95% confidence level.

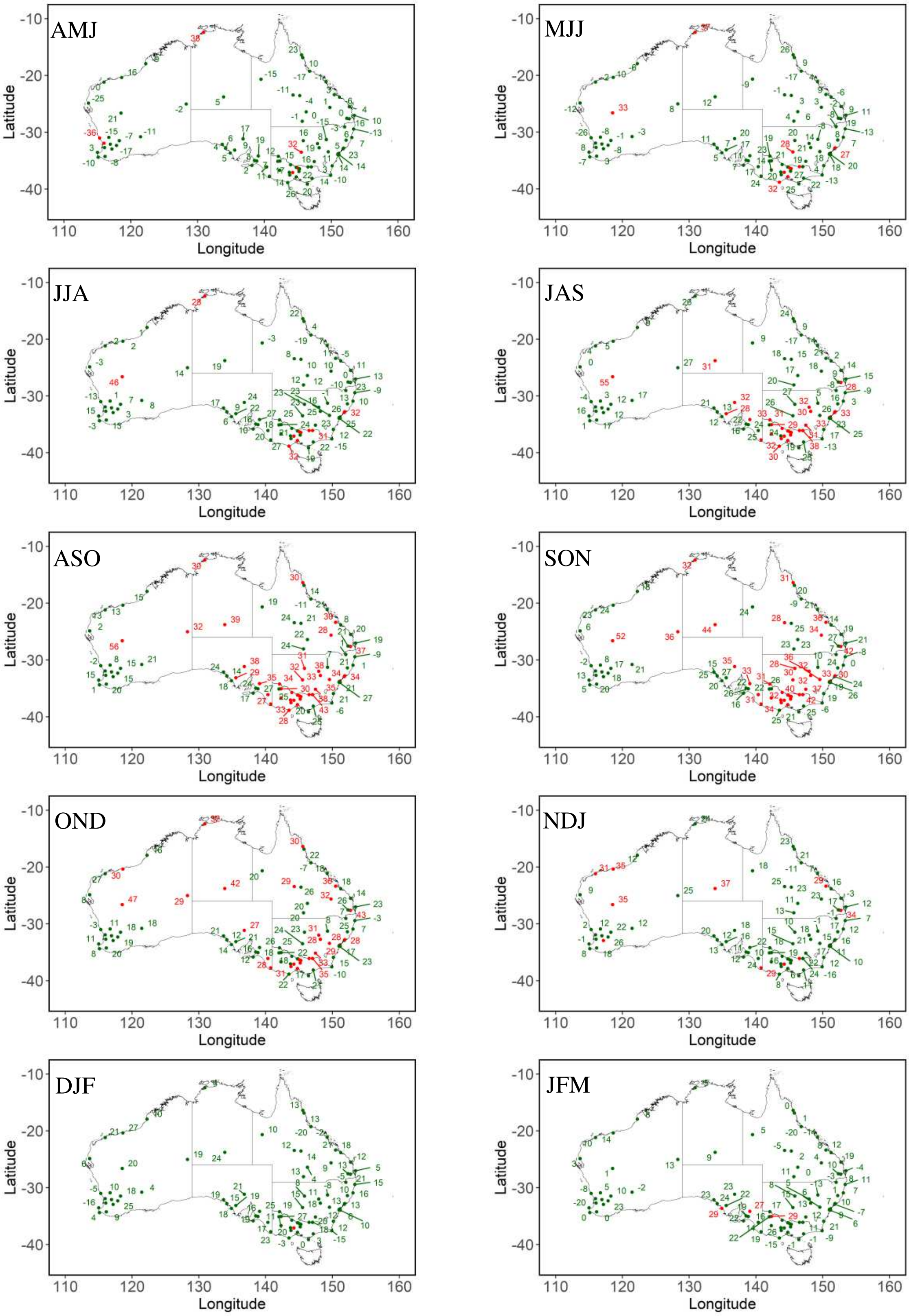

Figure 3. Spatial correlation of annual maximum temperature with IOD during 1969 – 2021. Correlation values are multiplied by 100, and red values are statistically significant at a 95% confidence level.

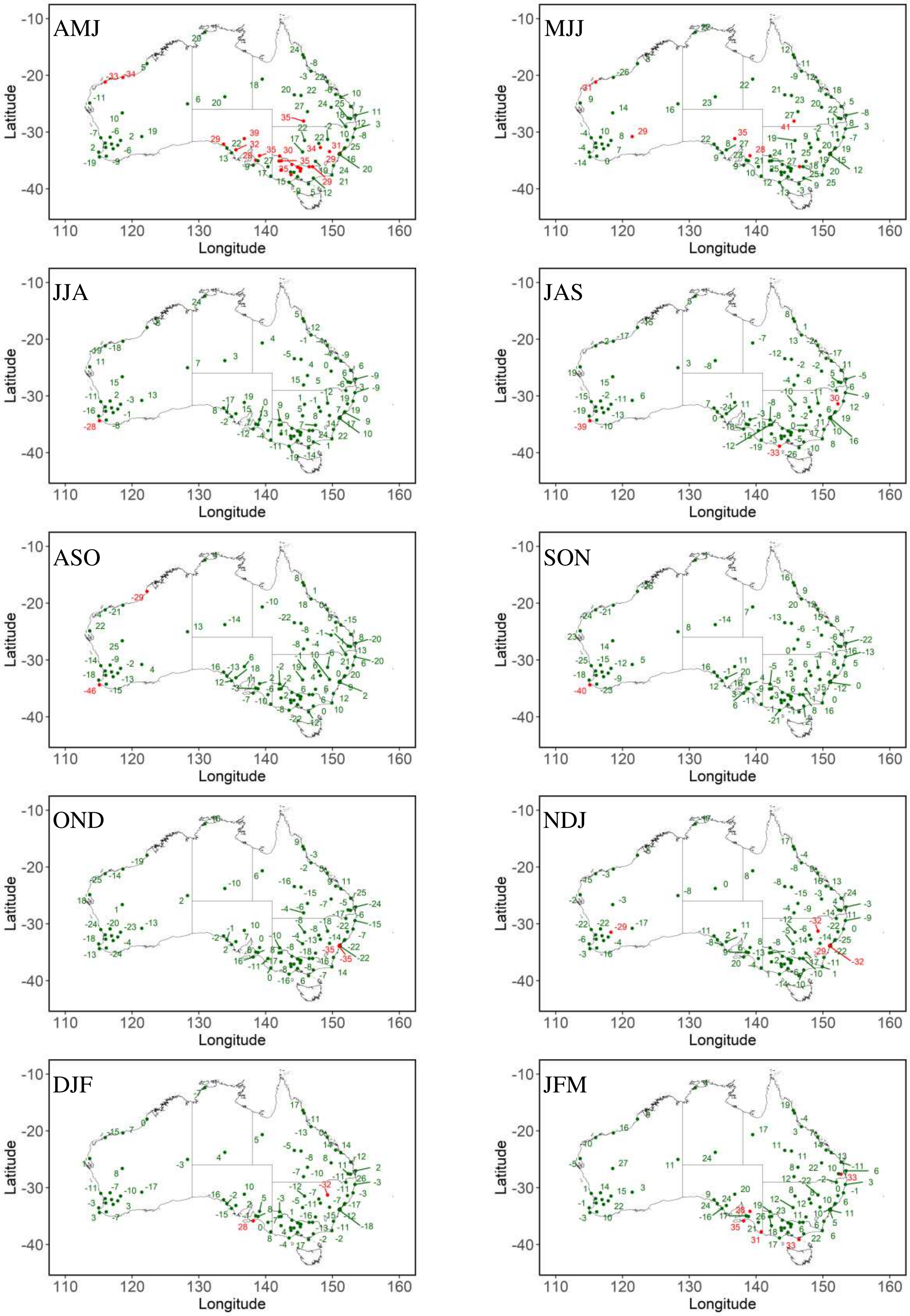

Figure 4. Spatial correlation of annual maximum temperature with SAM during 1969 – 2021. Correlation values are multiplied by 100, and red values are statistically significant at a 95% confidence level.

Considering the correlation values between the climate drivers averaged over different seasons and the temperature, one climate driver, was selected for each station along with the occurring season, as shown in Figure 5.

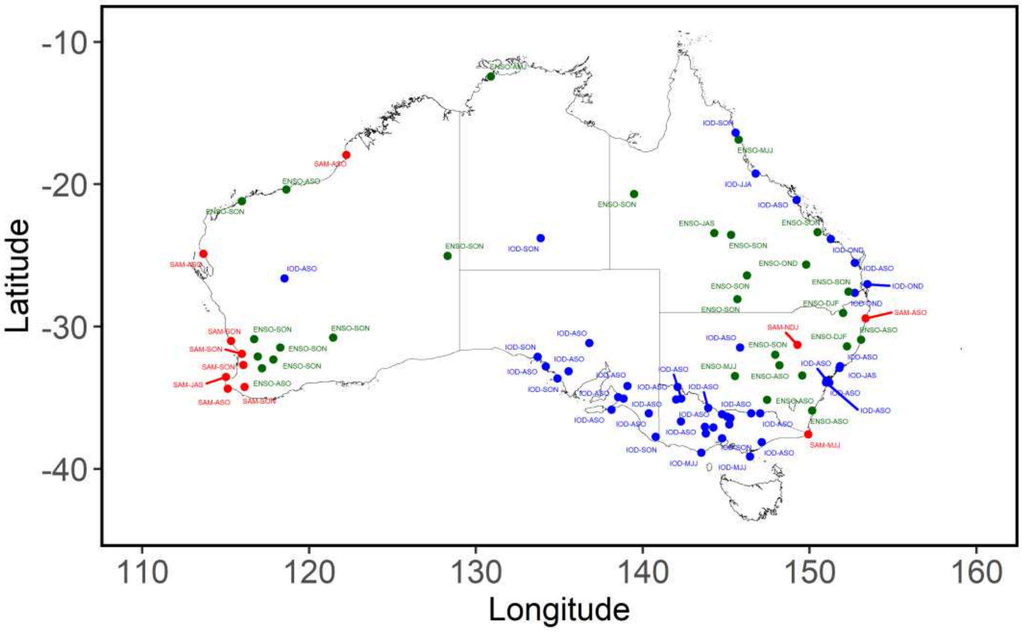

Figure 5. Selected climate drivers with season based on the correlations between annual maximum temperature and the climate drivers (ENSO, IOD and SAM) during 1969 – 2021.

One of the main findings of this study was that ENSO in spring acted as the dominant climate driver for the stations located in the inland NSW, Queensland and Western Australia, which is similar to the findings by a few other researchers (Min, Cai and Whetton, 2013). On the other hand, IOD had the strongest relations with temperature along the east coast and almost all stations in the coastal and inland regions of Victoria and South Australia. It should be noted that a significant decrease in rainfall across southern Australia as the frequency of positive IOD events has increased, which contributed to significant bushfires over southeastern regions of the continent (Cai, Cowan and Raupach, 2009; Cai, Cowan and Sullivan, 2009).

Although SAM in Autumn had strong relations with stations in NSW and Victoria, ENSO and IOD were the dominant climate drivers. Furthermore, one of the Department of Primary Industries and Regional Development studies reported a decline in rainfall due to SAM in southern Australia, particularly in the southwest region (Guthrie, 2021). However, SAM appeared as the selected climate driver at the stations located in the coastal regions of Western Australia. In the cases of stations located in the Northern Territory, the temperature recorded at the station on the coastal side was associated with ENSO, while at the inland, it was correlated with the IOD.

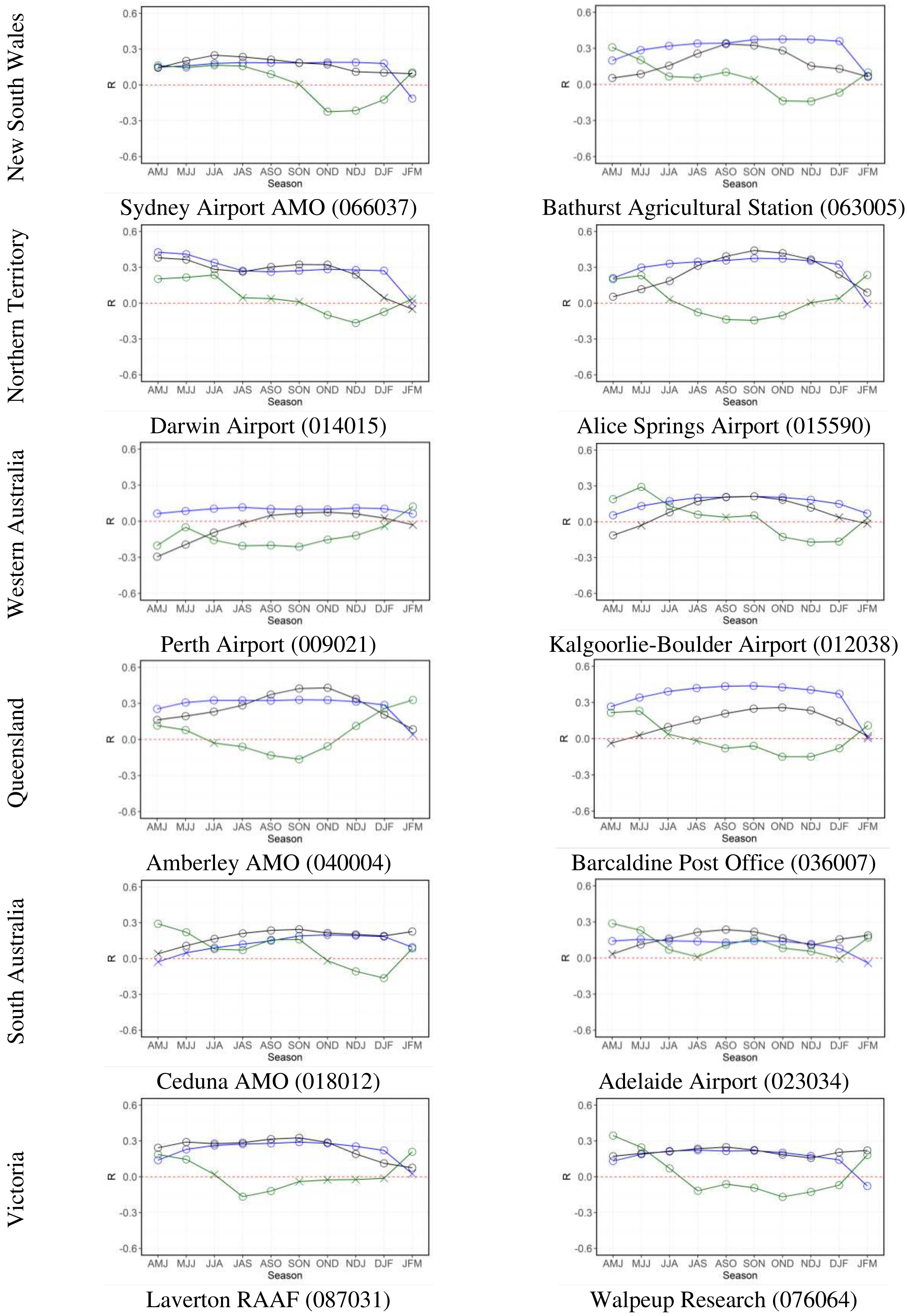

Figure 6. Correlations between annual maximum temperature and climate drivers. The blue, black and green lines represent correlations between AMT and ENSO, IOD and SAM, respectively.

Table 2. Pearson correlation coefficients between the annual maximum temperature series and the selected seasonal climate index

Station ID	Station Name	Latitude	Longitude	Climatic driver and season	Coefficient Value
066037	Sydney Airport AMO	-33.95	151.17	IOD(JJA)	0.25
063005	Bathurst Agricultural	-33.43	149.56	ENSO(SON)	0.37
014015	Darwin Airport	-12.42	130.89	ENSO(AMJ)	0.43
015590	Alice Springs Airport	-23.80	133.89	IOD(SON)	0.38
009021	Perth Airport	-31.93	115.98	SAM(SON)	-0.21
012038	Kalgoorlie-Boulder Airport	-30.78	121.45	SAM(MJJ)	0.29
040004	Amberley AMO	-27.63	152.71	IOD(OND)	0.43
036007	Barcaldine Post Office	-23.55	145.29	ENSO(SON)	0.44
018012	Ceduna AMO	-32.13	133.70	IOD(SON)	0.25
023034	Adelaide Airport	-34.95	138.52	IOD(ASO)	0.24
087031	Laverton RAAF	-37.86	144.76	IOD(SON)	0.33
076064	Walpeup Research	-35.12	142.00	IOD(ASO)	0.25

The Pearson correlation coefficient values for the annual maximum temperature series from April–May–June (AMJ) to January-February–March (JFM) of the same hydrological year recorded at 12 stations are presented in Figure 6. These illustrations validated the selection of the best climate drivers and seasons presented in Figure 5. Selected climate drivers with the seasons for the selected 12 stations are summarised in Table 2.

4.3 Stationary TDF

Figure 7 illustrates the stationary TDF curves based on GEV distribution as described in the methodology section. Estimated temperatures were plotted against the selected durations (1, 2, 3, 4, 5, 6, 7 and 10 days), with each curve indicating a different return period such as 2, 5, 10, 25, 50 and 100 years at station scale. These TDF curves demonstrated a significant rise in temperature with higher return periods and decreased with the increase in duration for all the selected stations.

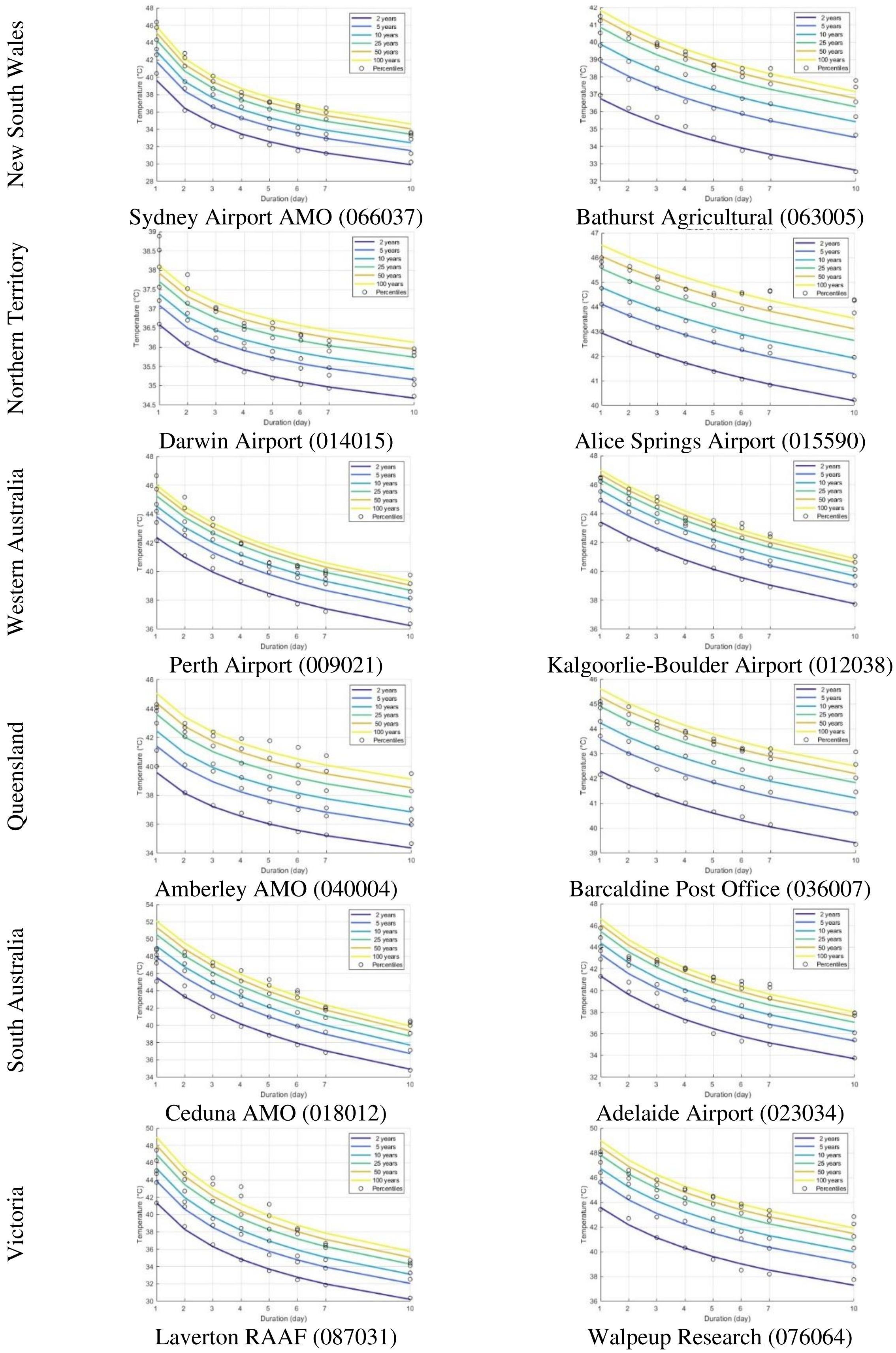

Figure 7. Stationary TDF curves for 2, 5, 10, 25, 50 and 100 years return periods.

4.1 Non-stationary TDF surfaces

For each TDF model and station, the maximal independence log-likelihood, the CL-AIC statistic, and the model parameters are summarised in Table 3. According to the values obtained by the AIC criterion from each model, the table only shows the optimal parameter relationship among the constant, linear and quadratic relationships to the covariate or the combinations of the covariates.

Table 3. Summary of parameters for the selected models and their error estimation.

Station	Model	l_{ind}	CL-AIC	Model parameters
Sydney Airport AMO	Stationary	-881.47	1791.45	μ, σ
	Time	-866.07	**1775.35**	$\mu_l = \mu_0 + \mu_1 T, \sigma$
	CD	-873.53	1787.97	$\mu_l = \mu_0 + \mu_1 I, \sigma$
	Time + CD	-863.46	1780.83	$\mu_l = \mu_0 + \mu_1 I + \mu_2 T, \sigma$
Bathurst Agricultural Station	Stationary	-939.29	1917.13	μ, σ
	Time	-851.05	1751.47	$\mu_l = \mu_0 + \mu_1 T, \sigma$
	CD	-895.64	1854.87	$\mu_l = \mu_0 + \mu_1 E + \mu_2 E^2, \sigma$
	***Time* + CD**	-808.35	**1692.00**	$\mu_l = \mu_0 + \mu_1 E + \mu_2 E^2 + \mu_3 T, \sigma$
Darwin Airport	Stationary	-324.62	676.26	μ, σ
	Time	-262.29	572.28	$\mu_l = \mu_0 + \mu_1 T + \mu_2 T^2, \sigma$
	CD	-287.11	625.63	$\mu_l = \mu_0 + \mu_1 E + \mu_2 E^2, \sigma$
	***Time* + CD**	-234.22	**525.28**	$\mu_l = \mu_0 + \mu_1 E + \mu_2 T + \mu_3 T^2, \sigma$
Alice Springs Airport	Stationary	-675.70	1390.62	μ, σ
	Time	-642.08	1358.22	$\mu_l = \mu_0 + \mu_1 T$ $\sigma_l = \sigma_0 + \sigma_1 T + \sigma_2 T^2$
	CD	-623.41	1304.61	$\mu_l = \mu_0 + \mu_1 I$ $\sigma_l = \sigma_0 + \sigma_1 I$
	***Time* + CD**	-621.70	**1304.38**	$\mu_l = \mu_0 + \mu_1 I + \mu_2 T, \sigma$
Perth Airport	Stationary	-763.95	1557.98	μ, σ
	Time	-763.95	1567.02	$\mu, \sigma_1 = \sigma_0 + \sigma_1 T$
	CD	-736.19	1526.39	$\mu_l = \mu_0 + \mu_1 S + \mu_2 S^2$ $\sigma_l = \sigma_0 + \sigma_1 S + \sigma_2 S^2$
	***Time* + CD**	-732.25	**1524.26**	$\mu_l = \mu_0 + \mu_1 S + \mu_2 S^2 + \mu_3 T$ $\sigma_l = \sigma_0 + \sigma_1 S + \sigma_2 T$
Kalgoorlie-Boulder Airport	Stationary	-791.51	1616.49	μ, σ
	Time	-774.88	1588.99	$\mu, \sigma_1 = \sigma_0 + \sigma_1 T$
	CD	-764.00	1582.79	$\mu_l = \mu_0 + \mu_1 S + \mu_2 S^2, \sigma$

Station	Model	l_{ind}	CL-AIC	Model parameters
	***Time* + CD**	-741.39	**1554.90**	$\mu_l = \mu_0 + \mu_1 S + \mu_2 S^2 + \mu_3 T$
				$\sigma_l = \sigma_0 + \sigma_1 S + \sigma_2 T$
Amberley AMO	Stationary	-844.36	1728.03	μ, σ
	Time	-798.10	1649.35	$\mu_l = \mu_0 + \mu_1 T, \sigma$
	CD	-806.68	1665.05	$\mu_l = \mu_0 + \mu_1 I, \sigma$
	***Time* + CD**	-779.77	**1623.46**	$\mu_l = \mu_0 + \mu_1 I + \mu_2 T, \sigma$
Barcaldine Post Office	Stationary	-733.20	1505.18	μ, σ
	Time	-721.59	1498.50	$\mu_l = \mu_0 + \mu_1 T, \sigma$
	CD	-635.98	**1344.19**	$\mu_l = \mu_0 + \mu_1 E + \mu_2 E^2$
				$\sigma_l = \sigma_0 + \sigma_1 E + \sigma_2 E^2$
	Time + CD	-628.05	1353.58	$\mu_l = \mu_0 + \mu_1 E + \mu_2 E^2 + \mu_3 T + \mu_4 T^2$
				$\sigma_l = \sigma_0 + \sigma_1 E + \sigma_2 T$
Ceduna AMO	Stationary	-934.32	1898.72	μ, σ
	Time	-924.77	1890.45	$\mu_l = \mu_0 + \mu_1 T, \sigma$
	CD	-919.05	1888.54	$\mu_l = \mu_0 + \mu_1 I + \mu_2 I^2, \sigma$
	Time + CD	-892.92	**1861.80**	$\mu_l = \mu_0 + \mu_1 I + \mu_2 I^2 + \mu_3 T + \mu_4 T^2$
				$\sigma_l = \sigma_0 + \sigma_1 I + \sigma_2 T$
Adelaide Airport	Stationary	-885.62	1803.53	μ, σ
	Time	-867.75	1790.75	$\mu_l = \mu_0 + \mu_1 T + \mu_2 T^2, \sigma$
	CD	-884.90	1810.97	$\mu, \sigma_l = \sigma_0 + \sigma_1 I$
	***Time* + CD**	-842.22	**1750.65**	$\mu_l = \mu_0 + \mu_1 I + \mu_2 T + \mu_3 T^2$
				$\sigma_l = \sigma_0 + \sigma_1 I + \sigma_2 T$
Laverton RAAF	Stationary	-939.13	1908.59	μ, σ
	Time	-931.24	**1902.91**	$\mu_l = \mu_0 + \mu_1 T, \sigma$
	CD	-932.31	1904.82	$\mu, \sigma_l = \sigma_0 + \sigma_1 I + \sigma_2 I^2$
	Time + CD	-922.50	1905.08	$\mu_l = \mu_0 + \mu_1 I + \mu_2 I^2 + \mu_3 T, \sigma$
Walpeup Research	Stationary	-915.68	1866.35	μ, σ
	Time	-864.87	1788.51	$\mu_l = \mu_0 + \mu_1 T + \mu_2 T^2, \sigma$
	CD	-908.46	1865.52	$\mu_l = \mu_0 + \mu_1 I, \sigma$
	***Time* + CD**	-846.70	**1772.17**	$\mu_l = \mu_0 + \mu_1 I + \mu_2 T + \mu_3 T^2$
				$\sigma_l = \sigma_0 + \sigma_1 I + \sigma_2 T$

* κ, θ, η are constant for all models.

T = *Time*, E = ENSO, I = IOD, S = SAM

The CL-AIC statistic and log-likelihood suggested that the *Time* and covariate individually or combinedly increased the goodness-of-fit compared to the stationary model for all the stations. It's worth noting that employing a non-stationary model or the GEV enhances the log-likelihood in every case. However, the performances of different stationary and non-stationary TDF models were compared by the CL –AIC values, which were penalised due to the inclusion of more variables and thereby provided more reliable results.

Most stations (9 out of 12) with a combination of *Time* and Climatic Drivers (CD) as covariates showed the best goodness-of-fit. This suggested that the combination of the two covariates considerably impacted severe temperatures. *Time* was more prominent than climate drivers and qualified as the best covariate in cases of Sydney Airport AMO and Laverton RAAF stations. On the other hand, for Barcaldine Post Office, the influence of covariate alone was stronger than *Time* or the combination of *Time* and climate driver as the covariate.

i. Non-stationary TDF surfaces – One covariate (Time or Climate driver)

Figures 8 and 9 present the non-stationary TDF graphs with the model considering *Time* and climate driver as a covariate for the typical stations. For all the illustrated stations in this study, non-stationary TDF models with *Time* as a covariate, either scale or location parameters were found to be varied linearly with time, except for Darwin, Alice Springs Airport, Adelaide Airport, Walpeup Research, where either of the parameters varied quadratically with time. TDF curves with *Time* as a covariate for Kalgoorlie-Boulder Airport stations linearly varied with time but were not parallel to each other for different return periods. In the case of Perth stations, the estimated temperature increased with return periods and decreased with duration but did not vary significantly with time. However, in the case of non-stationary TDF models with climate drivers as covariates, the scale or location parameters varied quadratically with selected climate drivers for most stations.

Consequently, the TDF curves varied parabolically with climate drivers. Exceptions were observed for Sydney Airport AMO, Alice Spring Airport, Amberly AMO, Adelaide Airport and Walpeup Research stations, where either scale or the location parameter changed linearly with climate drivers and exhibited linear TDF curves for different return periods and durations. These characteristics of non-stationary TDF models can be seen distinctively in Figures S2 – S5 (in supplementary sections).

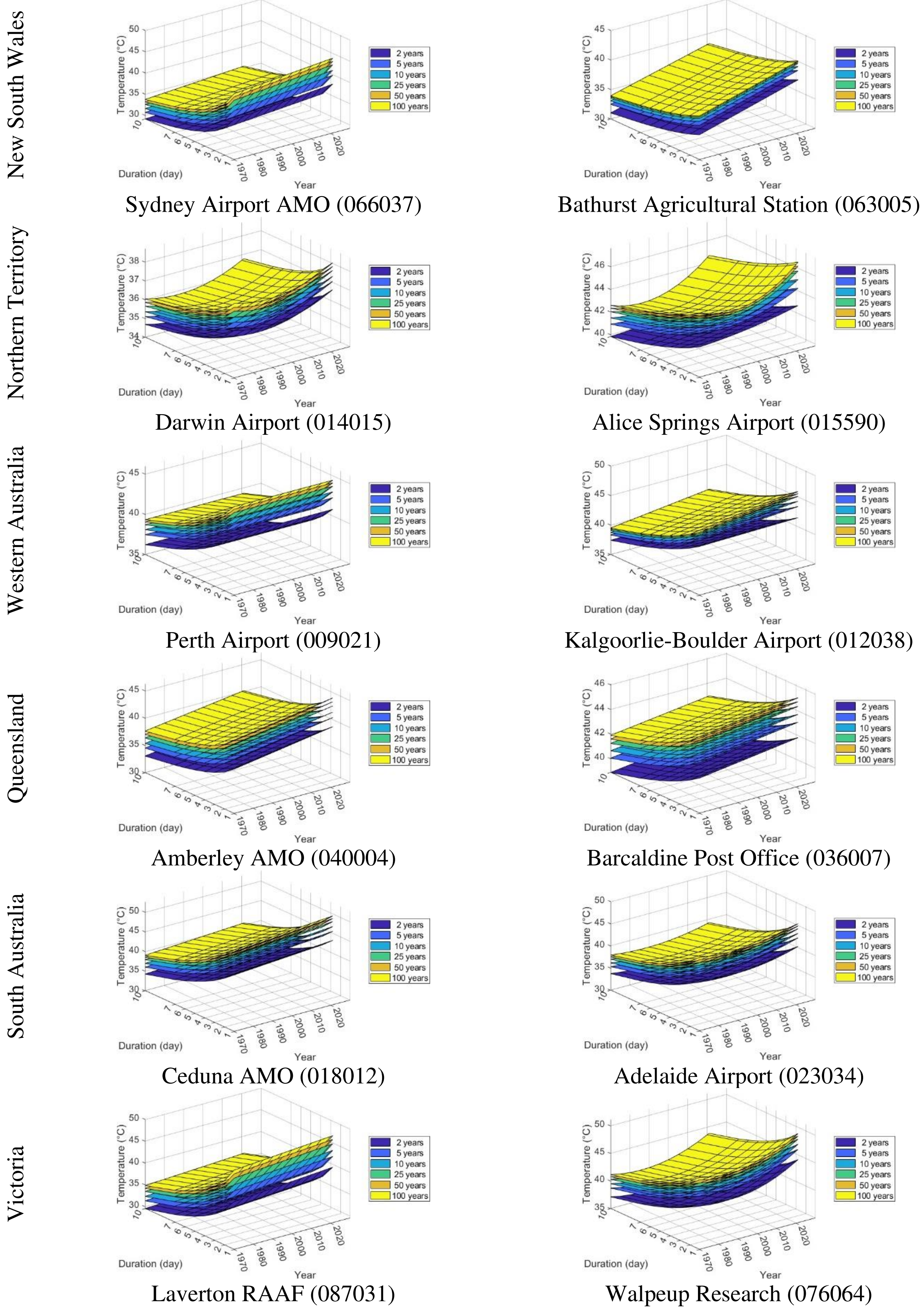

Figure 8. Non-stationary TDF surfaces with *Time* covariates for 2, 5, 10, 25, 50 and 100 years return periods.

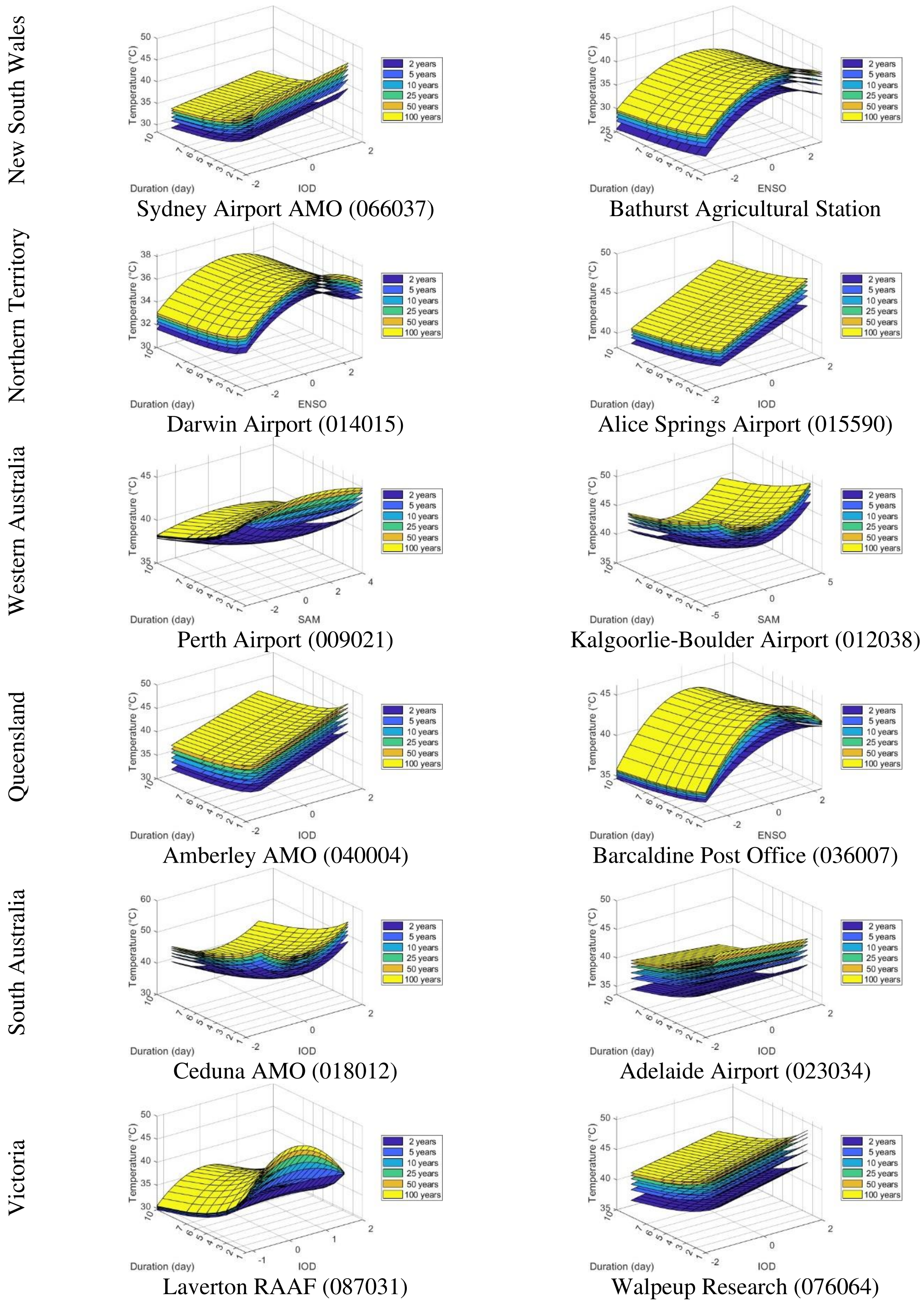

Figure 9. Non-stationary TDF surfaces with climate driver covariates for 2, 5, 10, 25, 50 and 100 years return periods.

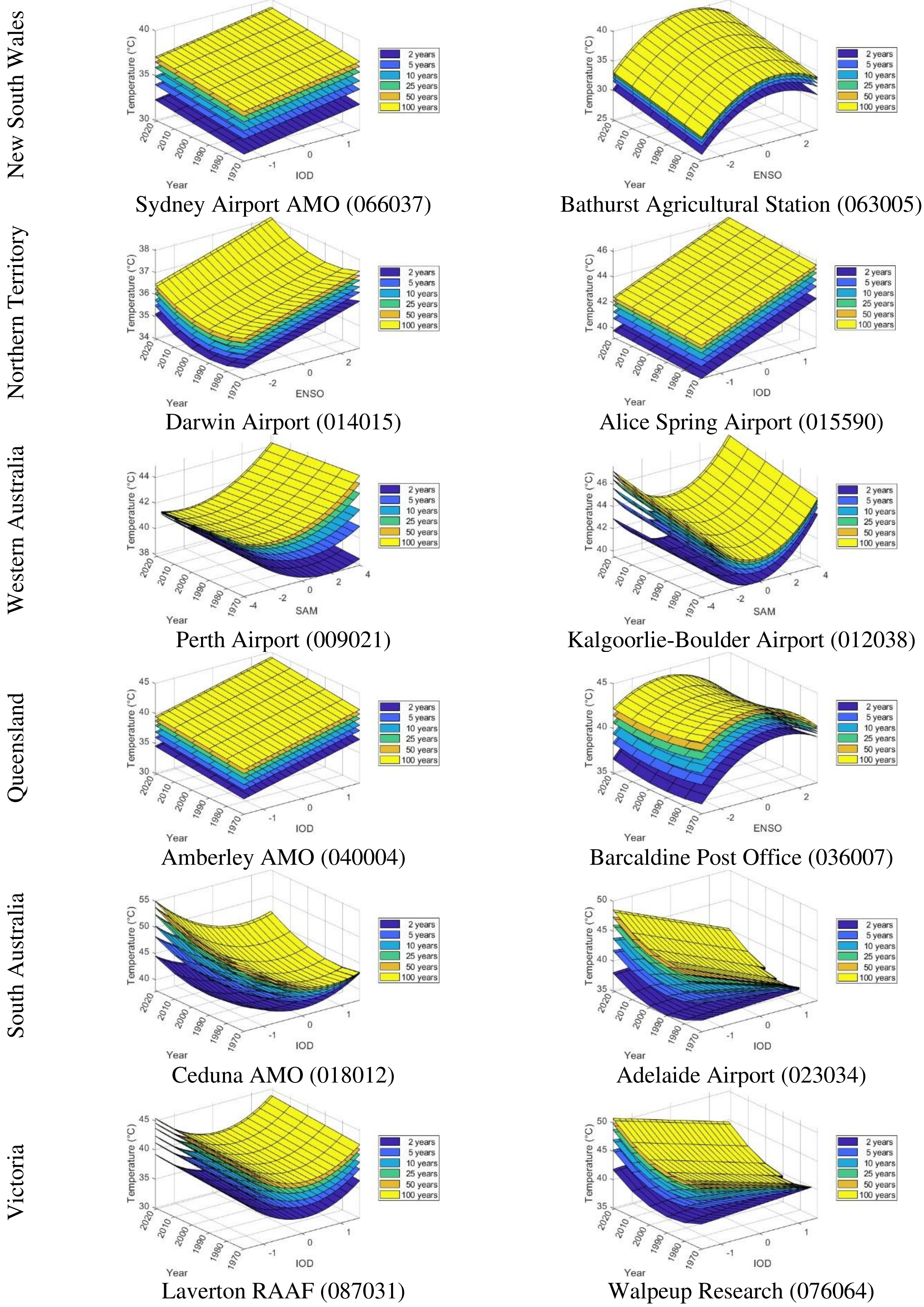

Figure 10. Non-stationary TDF surfaces with *Time* and climate driver as covariates of 5-days duration for 2, 5, 10, 25, 50 and 100 years return periods.

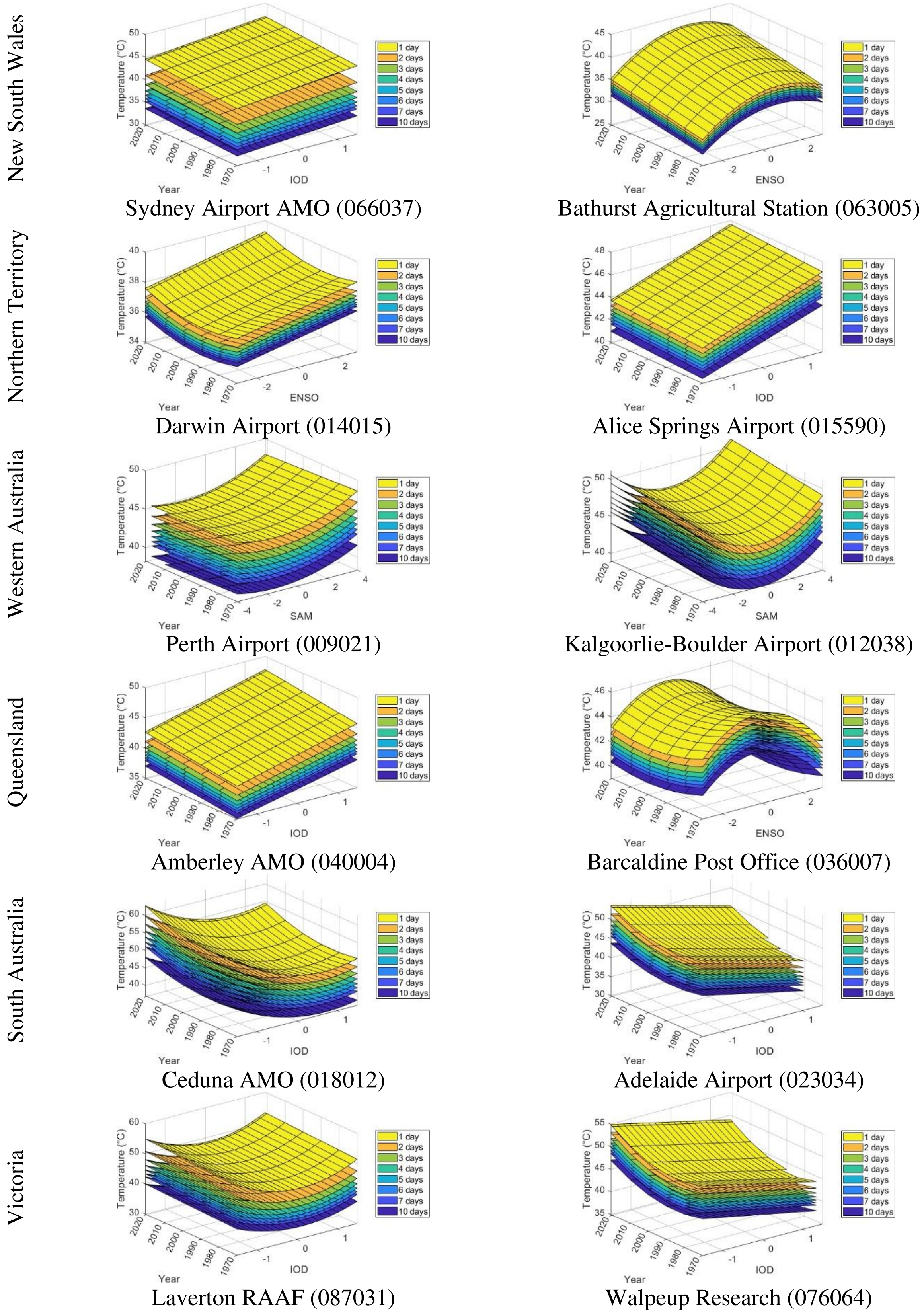

Figure 11. Non-stationary TDF surfaces with *Time* and climate driver as covariates of 50-year return period for 1, 2, 3, 4, 5, 6, 7 and 10 days durations.

ii. Non-stationary TDF surfaces – Two covariates (Time and Climate Drivers as covariates)

For non-stationary TDF models incorporating two covariates, five variables are required to be present in the graph. Therefore, in this paper, non-stationary TDF surfaces are presented in two ways – either the duration is kept fixed and TDF surfaces for different return periods are presented, or return period is kept fixed and TDF surfaces for different durations are illustrated. Figure 10 shows the TDF surfaces for 5-day duration and all the return periods considered in this study, whereas Figure 11 presents the TDF surfaces for 50-year return period and all the considered durations.

4.2 Impacts of non-stationarity on TDF curves

The temperature quantiles calculated at a given time are significantly affected by incorporating one or more covariates. Figure 12 shows the graphs of the 50-year quantiles versus the duration for the stationary TDF model and the non-stationary TDF models considering different *Time* and covariates representing different scenarios for each station. The non-stationary quantiles for the first and last years of the study period were computed with *Time* covariate and denoted as *Time* (1970) and *Time* (2021) to display the quantiles' temporal movement. The years with the highest and lowest values of the selected seasonal climatic drivers throughout the period 1970 – 2021 were selected for "CD" and "*Time* + CD" non-stationary models to highlight the influence of the extreme conditions on the estimated quantiles. All the graphs illustrated in Figure 12 use the model that provides the greatest overall fit.

In all stations, it was observed that the influence of the duration on the difference in quantile estimation between the stationary and non-stationary models was negligible. For all the 12 stations, the stationary model always overestimated and underestimated the return levels in the case of the non-stationary models with the earliest (1970) and latest (2021) years of the study period as *Time* covariate, respectively. The stationary model overestimated upto 4.2 °C compare to the former cases, while underestimated upto 2.3 °C for the latter cases at all 12 stations. The only exception was for the Perth Airport station, where *Time* covariate had no significant influence. This can be explained by the fact that the Perth Airport station showed no non-stationarity (Table 1) and no temporal trend in the annual maximum temperature during the study period (Figure S1).

In general, for all the stations, the difference between the stationary and non-stationary models incorporating the climate drivers as covariates decreased with the return period, as shown in Figures S6 – S10. Also, the stations where IOD was selected as the climate driver showed a significant difference between stationary and non-stationary models compared to the other stations where ENSO and SAM were selected as the climate drivers.

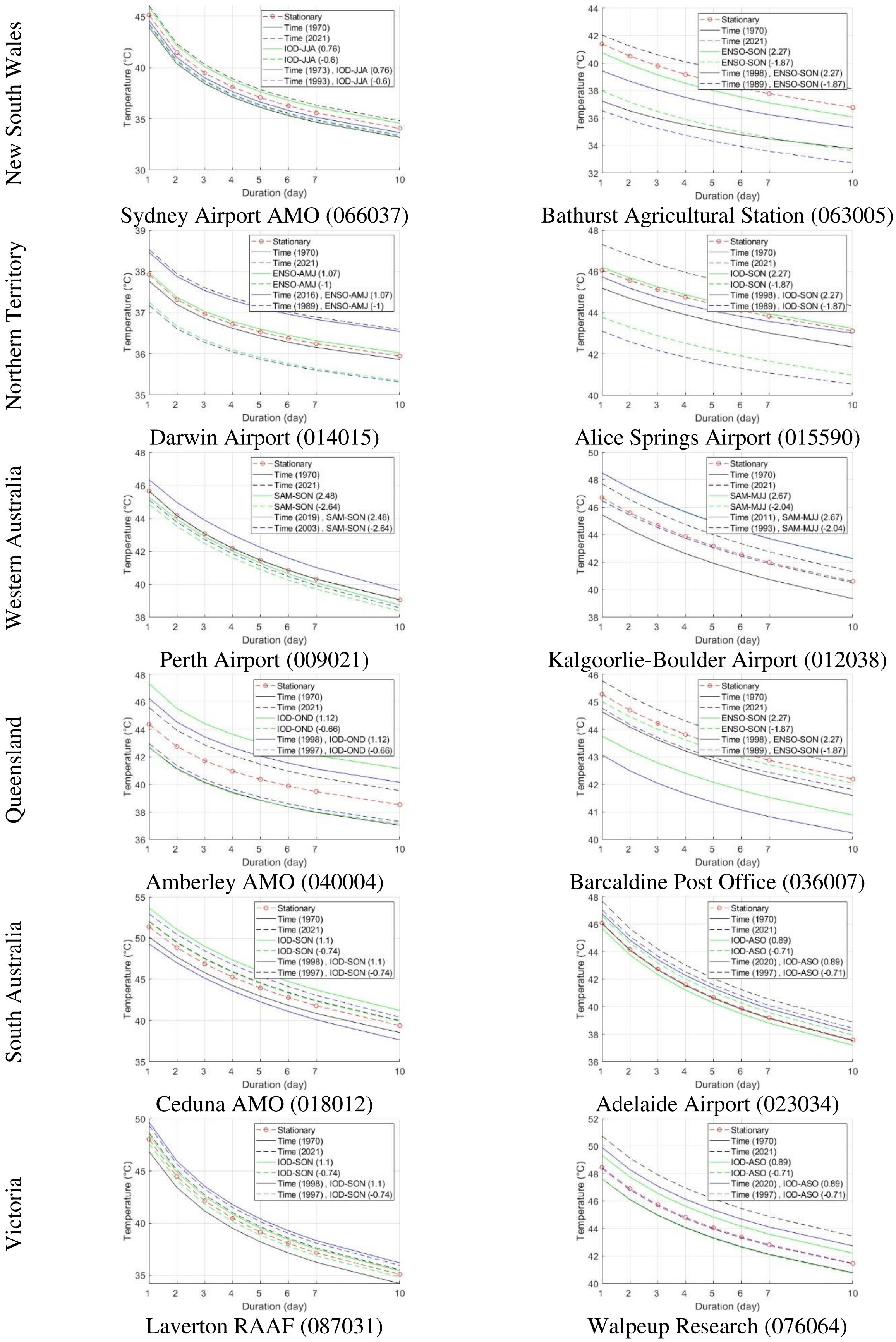

Figure 12. Comparison between stationary and non-stationary TDF curves (50-year quantiles).

The average difference between the stationary model and the non-stationary models considering the climate driver alone as covariate ranged from -3.0 to 1.5 °C (+ CD) and -0.6 to 3.4 °C (– CD). In contrast, this difference became -1.9 to 2.2 °C ("*Time* + CD") and -1.6 to 4.7°C ("*Time* – CD") in the case of the combination of two covariates – *Time* and selected climate driver.

Although *Time* had the overall dominance as a covariate on the computed quantiles for all the return periods compared to the selected climate indices, different covariates or combinations of them yielded the maximum quantiles for different return periods and stations.

5. CONCLUSION

In this study, the formulation of stationary and non-stationary TDF curves was based on temperature time series from 82 weather stations located in Australia using the GEV distribution. Initially, the augmented Dickey-Fuller (ADF) test was conducted to identify non-stationarity in temperature time series and non-stationarity was found to be present in the data series.

The long-range relationships between the seasonal climate drivers ENSO, IOD, SAM and temperature data from 1969 to 2021 were investigated using the Pearson correlation coefficient to find out the best covariates in non-stationary TDF models. The magnitude of correlation coefficients of ENSO increases towards the east of Australia, and these coefficients are significant during SON and DJF seasons. The annual maximum temperature observed at stations in the southeastern region of Australia, especially in the inland and coastal region of Victoria and South Australia, showed a significant correlation with IOD during SON. SAM showed a strong correlation with the annual temperature at the stations located in the coastal regions of Western Australia

Stationary TDF curves showed an increase and decrease in design temperatures with higher return periods and an increase in duration, respectively. In the case of non-stationary TDF models, the location and scale parameters were modelled as being dependent on time and climate indicators for the selected stations. Inclusion of the selected covariates in non-stationary TDF models enhanced goodness-of-fit compared to the stationary TDF model for the corresponding station. Similar results were found by Ouarda and Charron (2018a) where the influence of the climate oscillation pattern was found to be more prominent than the temporal trend. Furthermore, the best goodness-of-fit of the TDF model based on the AIC values was obtained with a combination of both covariates *Time* and selected climate driver for most of the stations. These results highlighted the importance of considering the combined effect of the temporal trend caused by global warming and climate drivers in statistical models used to predict design temperature.

The non-stationary quantiles computed with the first and last years of the study period and with the highest and lowest values of the selected seasonal climatic drivers were compared with the stationary model to display the quantiles' temporal movement and the influence of the extreme conditions on the quantiles. In most cases, the stationary TDF model underestimated the design temperature compared to the non-stationary model, including *Time* as a covariate. This conveys a crucial message that the non-stationary framework for designing temperature facilities in Australia could be considered a stronger option than the traditional stationary approach. In addition, TDF curves developed in this study can be applied to a range of sectors such as agriculture, health care and energy production and can be a useful tool for policymakers and planners.

Data availability

The data used in this study can be obtained by contacting the Australian Bureau of Meteorology (by paying a prescribed fee) (Australia's official weather forecasts & weather radar - Bureau of Meteorology (bom.gov.au)). Nino3.4 and DMI data used in this study can be obtained freely from NOAA (https://psl.noaa.gov/gcos_wgsp/Timeseries/Nino34/) and (https://psl.noaa.gov/gcos_wgsp/Time series /DMI/; and SAM data has been obtained from NERC (http://www.nerc-bas.ac.uk/ icd/gjma/sam.html).

6. REFERENCE

Adlouni, S. El and Ouarda, T. B. M. J. (2009) 'Joint Bayesian model selection and parameter estimation of the generalized extreme value model with covariates using birth-death Markov chain Monte Carlo', *Water Resources Research*, 45(6), pp. 1–11. doi: 10.1029/2007WR006427.

Arblaster, J. M. and Alexander, L. V. (2012) 'The impact of the El Nio-Southern Oscillation on maximum temperature extremes', *Geophysical Research Letters*, 39(20), pp. 2–6. doi: 10.1029/2012GL053409.

Bellenger, H. *et al.* (2014) 'ENSO representation in climate models: From CMIP3 to CMIP5', *Climate Dynamics*, 42(7–8), pp. 1999–2018. doi: 10.1007/s00382-013-1783-z.

Berghuijs, W. R. *et al.* (2019) 'Growing Spatial Scales of Synchronous River Flooding in Europe', *Geophysical Research Letters*, 46(3), pp. 1423–1428. doi: 10.1029/2018GL081883.

Boschat, G. *et al.* (2015) 'Large scale and sub-regional connections in the lead up to summer heat wave and extreme rainfall events in eastern Australia', *Climate Dynamics*, 44(7–8), pp. 1823–1840. doi: 10.1007/s00382-014-2214-5.

Cai, W. *et al.* (2011) ‘Teleconnection pathways of ENSO and the IOD and the mechanisms for impacts on Australian rainfall’, *Journal of Climate*, 24(15), pp. 3910–3923. doi: 10.1175/2011JCLI4129.1.

Cai, W. *et al.* (2014) ‘Increasing frequency of extreme El Niño events due to greenhouse warming’, *Nature Climate Change*, 4(2), pp. 111–116. doi: 10.1038/nclimate2100.

Cai, W., Cowan, T. and Raupach, M. (2009) ‘Positive Indian Ocean Dipole events precondition southeast Australia bushfires’, 36(October), pp. 1–6. doi: 10.1029/2009GL039902.

Cai, W., Cowan, T. and Sullivan, A. (2009) ‘Recent unprecedented skewness towards positive Indian Ocean Dipole occurrences and its impact on Australian rainfall’, *Geophysical Research Letters*, 36(11), pp. 1–5. doi: 10.1029/2009GL037604.

Cai, W. and Van Rensch, P. (2012) ‘The 2011 southeast Queensland extreme summer rainfall: A confirmation of a negative Pacific Decadal Oscillation phase?’, *Geophysical Research Letters*, 39(8), pp. 1–7. doi: 10.1029/2011GL050820.

Cheng, L. *et al.* (2014) ‘Non-stationary extreme value analysis in a changing climate’, *Climatic Change*, 127(2), pp. 353–369. doi: 10.1007/s10584-014-1254-5.

Cheng, L. and Aghakouchak, A. (2014) ‘Nonstationary precipitation intensity-duration-frequency curves for infrastructure design in a changing climate’, *Scientific Reports*, 4, pp. 1–6. doi: 10.1038/srep07093.

Chowdary, J. S., John, N. and Gnanaseelan, C. (2014) ‘Interannual variability of surface air-temperature over India: Impact of ENSO and Indian Ocean Sea surface temperature’, *International Journal of Climatology*, 34(2), pp. 416–429. doi: 10.1002/joc.3695.

Coles, S. (2001) *An introduction to statistical modeling of extreme values*. Springer.

Cowan, T. *et al.* (2014) ‘More frequent, longer, and hotter heat waves for Australia in the Twenty-First Century’, *Journal of Climate*, 27(15), pp. 5851–5871. doi: 10.1175/JCLI-D-14-00092.1.

CSIRO and Australian Government (Bureau of Meteorology) (2020) ‘State of the Climate 2020: Australia’s changing climate’, *Medicine*, pp. 1–24. Available at: https://apo.org.au/node/309418.

Devi, R., Gouda, K. C. and Lenka, S. (2022) ‘Temperature-duration-frequency analysis over Delhi and Bengaluru city in India’, *Theoretical and Applied Climatology*, 147(1–2), pp. 291–305. doi: 10.1007/s00704-021-03824-5.

Galiatsatou, P. and Iliadis, C. (2022) ‘Intensity-Duration-Frequency Curves at Ungauged Sites in a Changing Climate for Sustainable Stormwater Networks’, *Sustainability (Switzerland)*, 14(3), pp. 1–24. doi: 10.3390/su14031229.

Ganguli, P. and Coulibaly, P. (2017) ‘Does nonstationarity in rainfall require nonstationary intensity-duration-frequency curves?’, *Hydrology and Earth System Sciences*, 21(12), pp. 6461–6483. doi: 10.5194/hess-21-6461-2017.

Guthrie, M. (2021) *Climate drivers of the South West Land Division*. Available at: https://www.agric.wa.gov.au/climate-weather/climate-drivers-south-west-land-division (Accessed: 9 June 2022).

Haddad, K. (2021) ‘Selection of the best fit probability distributions for temperature data and the use of L-moment ratio diagram method: a case study for NSW in Australia’, *Theoretical and Applied Climatology*, 143(3–4), pp. 1261–1284. doi: 10.1007/s00704-020-03455-2.

Halpert, M. S. and Ropelewski, C. F. (1992) ‘Surface Temperature Patterns Associated with the Southern Oscillation’, *Journal of Climate*, pp. 577–593. doi: 10.1175/1520-0442(1992)005<0577:stpawt>2.0.co;2.

Hendon, H. H., Thompson, D. W. J. and Wheeler, M. C. (2007) ‘Australian rainfall and surface temperature variations associated with the Southern Hemisphere annular mode’, *Journal of Climate*, 20(11), pp. 2452–2467. doi: 10.1175/JCLI4134.1.

Hundecha, Y. *et al.* (2008) ‘A nonstationary extreme value analysis for the assessment of changes in extreme annual wind speed over the gulf of St. Lawrence Canada’, *Journal of Applied Meteorology and Climatology*, 47(11), pp. 2745–2759. doi: 10.1175/2008JAMC1665.1.

IPCC (2018) *Summary for Policymakers. In: Global warming of 1.5°C. An IPCC Special Report on the impacts of global warming of 1.5°C above pre-industrial levels and related global greenhouse gas emission pathways, in the context of strengthening the global response to*, *World Meteorological Organization, Geneva, Switzerland*. Geneva, Switzerland. doi: 10.1017/CBO9781107415324.

Katz, R. W., Parlange, M. B. and Naveau, P. (2002) ‘Statistics of extremes in hydrology’, *Advances in Water Resources*, 25(8–12), pp. 1287–1304. doi: 10.1016/S0309-1708(02)00056-8.

Koutsoyiannis, D., Kozonis, D. and Manetas, A. (1998) ‘A mathematical framework for studying rainfall intensity-duration-frequency relationships’, *Journal of Hydrology*, 206(1–2), pp. 118–135. doi:

10.1016/S0022-1694(98)00097-3.

Kwon, H.-H. and Lall, U. (2016) ‘A copula-based nonstationary frequency analysis for the 2012-2015 drought in California’, *Water Resources Research*, 52(7), pp. 5662–5675. doi: 10.1002/2016WR018959.

Liu, L. *et al.* (2014) ‘Indian Ocean variability in the CMIP5 multi-model ensemble: The zonal dipole mode’, *Climate Dynamics*, 43(5–6), pp. 1715–1730. doi: 10.1007/s00382-013-2000-9.

Lorenz, R., Stalhandske, Z. and Fischer, E. M. (2019) ‘Detection of a Climate Change Signal in Extreme Heat, Heat Stress, and Cold in Europe From Observations’, *Geophysical Research Letters*, 46(14), pp. 8363–8374. doi: 10.1029/2019GL082062.

Maher, P. and Sherwood, S. C. (2014) ‘Disentangling the multiple sources of large-scale variability in Australian wintertime precipitation’, *Journal of Climate*, 27(17), pp. 6377–6392. doi: 10.1175/JCLI-D-13-00659.1.

Meyers, G. *et al.* (2007) ‘The years of El Niño, La Niña and interactions with the tropical Indian Ocean’, *Journal of Climate*, 20(13), pp. 2872–2880. doi: 10.1175/JCLI4152.1.

Min, S. K., Cai, W. and Whetton, P. (2013) ‘Influence of climate variability on seasonal extremes over Australia’, *Journal of Geophysical Research Atmospheres*, 118(2), pp. 643–654. doi: 10.1002/jgrd.50164.

Nicholls, N. (1985) ‘Towards the prediction of major Australian droughts.’, *Australian Meteorological Magazine*, 33, pp. 161–166.

Nicholls, N. and Lucas, C. (2007) ‘Interannual variations of area burnt in Tasmanian bushfires: Relationships with climate and predictability’, *International Journal of Wildland Fire*, 16(5), pp. 540–546. doi: 10.1071/WF06125.

Oliveira, F. N. M. and Ambrizzi, T. (2017) ‘The effects of ENSO-types and SAM on the large-scale southern blockings’, *International Journal of Climatology*, 37(7), pp. 3067–3081. doi: 10.1002/joc.4899.

Omer, A. *et al.* (2020) ‘Natural and anthropogenic influences on the recent droughts in Yellow River Basin, China’, *Science of the Total Environment*, 704. doi: 10.1016/j.scitotenv.2019.135428.

Ouarda, T. B. M. J. and Charron, C. (2018a) ‘Nonstationary Temperature-Duration-Frequency curves’, *Scientific Reports*, 8(1), pp. 1–8. doi: 10.1038/s41598-018-33974-y.

Ouarda, T. B. M. J. and Charron, C. (2018b) 'Nonstationary Temperature-Duration-Frequency curves', *Scientific Reports*, 8(1), pp. 1–8. doi: 10.1038/s41598-018-33974-y.

Ouarda, T. B. M. J., Charron, C. and St-Hilaire, A. (2020) 'Uncertainty of stationary and nonstationary models for rainfall frequency analysis', *International Journal of Climatology*, 40(4), pp. 2373–2392. doi: 10.1002/joc.6339.

Ouarda, T. B. M. J., Yousef, L. A. and Charron, C. (2019) 'Non-stationary intensity-duration-frequency curves integrating information concerning teleconnections and climate change', *International Journal of Climatology*, 39(4), pp. 2306–2323. doi: 10.1002/joc.5953.

Parker, T. J., Berry, G. J. and Reeder, M. J. (2013) 'The influence of tropical cyclones on heat waves in Southeastern Australia', *Geophysical Research Letters*, 40(23), pp. 6264–6270. doi: 10.1002/2013GL058257.

Perkins, S. E., Argüeso, D. and White, C. J. (2015) 'Relationships between climate variability, soil moisture, and Australian heatwaves', *Journal of Geophysical Research: Atmospheres*, 120(16), pp. 8144–8164. doi: 10.1002/2015JD023592.

Power, S. *et al.* (1999) 'Inter-decadal modulation of the impact of ENSO on Australia', *Climate Dynamics*, 15(5), pp. 319–324. doi: 10.1007/s003820050284.

Power, S. B. *et al.* (2006) 'The Predictability of Interdecadal Changes in ENSO Activity and ENSO Teleconnections', *Journal of Climate*, 19(19), pp. 4755–4771.

Risbey, J. S. *et al.* (2009) 'On the remote drivers of rainfall variability in Australia', *Monthly Weather Review*, 137(10), pp. 3233–3253. doi: 10.1175/2009MWR2861.1.

Ropelewski, C. F. and Halpert, M. S. (1988) 'Precipitation Patterns Associated with the High Index Phase of the Southern Oscillation', *Journal of Climate*, 2(3), pp. 268–284.

Rossi, F. and Villani, P. (1994) 'A project for regional analysis of floods in Italy', in Rossi, G., Harmancio\uglu, N., and Yevjevich, V. (eds) *Coping with Floods*. Dordrecht: Springer Netherlands, pp. 193–217. doi: 10.1007/978-94-011-1098-3_11.

Saji, N. H. *et al.* (1999) 'A dipole mode in the tropical Indian ocean', *Nature*, 401(6751), pp. 360–363. doi: 10.1038/43854.

Sarhadi, A. and Soulis, E. D. (2017) ‘Time-varying extreme rainfall intensity-duration-frequency curves in a changing climate’, *Geophysical Research Letters*, 44(5), pp. 2454–2463. doi: 10.1002/2016GL072201.

Sein, K. K., Chidthaisong, A. and Oo, K. L. (2018) ‘Observed trends and changes in temperature and precipitation extreme indices over Myanmar’, *Atmosphere*, 9(12). doi: 10.3390/atmos9120477.

Spinoni, J., Naumann, G. and Vogt, J. V. (2017) ‘Pan-European seasonal trends and recent changes of drought frequency and severity’, *Global and Planetary Change*, 148, pp. 113–130. doi: 10.1016/j.gloplacha.2016.11.013.

Sugahara, S., da Rocha, R. P. and Silveira, R. (2009) ‘Non-stationary frequency analysis of extreme daily rainfall in Sao Paulo, Brazil’, *International Journal of Climatology*, 29(9), pp. 1339–1349. doi: 10.1002/joc.1760.

Suman, M. and Maity, R. (2020) ‘Southward shift of precipitation extremes over south Asia: Evidences from CORDEX data’, *Scientific Reports*, 10(1), pp. 1–11. doi: 10.1038/s41598-020-63571-x.

Thompson, D. W. J., Wallace, J. M. and Hegerl, G. C. (2000) ‘Annular Modes in the Extratropical Circulation . Part II : Trends Author (s): David W . J . Thompson , John M . Wallace and Gabriele C . Hegerl Published by : American Meteorological Society Stable URL : https://www.jstor.org/stable/10.2307/26244740 REF’, 13(5), pp. 1018–1036.

Turney, C. S. M. *et al.* (2007) ‘Quaternary climatic, environmental and archaeological change in Australasia’, *Journal of Quaternary Science*, 22(5), pp. 421–422. doi: 10.1002/jqs.1139.

Ummenhofer, C. C. *et al.* (2009) ‘What causes southeast Australia’s worst droughts?’, *Geophysical Research Letters*, 36(4), pp. 1–6. doi: 10.1029/2008GL036801.

Ummenhofer, C. C. *et al.* (2011) ‘Indian and Pacific Ocean influences on southeast Australian drought and soil moisture’, *Journal of Climate*, 24(5), pp. 1313–1336. doi: 10.1175/2010JCLI3475.1.

Wang, X. L. *et al.* (2013) ‘Historical changes in Australian temperature extremes as inferred from extreme value distribution analysis’, *Geophysical Research Letters*, 40(3), pp. 573–578. doi: 10.1002/grl.50132.

White, C. J. *et al.* (2013) ‘On regional dynamical downscaling for the assessment and projection of temperature and precipitation extremes across Tasmania, Australia’, *Climate Dynamics*, 41(11–12), pp.

3145–3165. doi: 10.1007/s00382-013-1718-8.

Yan, H. *et al.* (2019) 'Next-Generation Intensity–Duration–Frequency Curves to Reduce Errors in Peak Flood Design', *Journal of Hydrologic Engineering*, 24(7), p. 04019020. doi: 10.1061/(asce)he.1943-5584.0001799.

Yan, H. *et al.* (2020) 'Evaluating next-generation intensity–duration–frequency curves for design flood estimates in the snow-dominated western United States', *Hydrological Processes*, 34(5), pp. 1255–1268. doi: 10.1002/hyp.13673.

Yilmaz, A. G. and Perera, B. J. C. (2014) 'Extreme Rainfall Nonstationarity Investigation and Intensity–Frequency–Duration Relationship', *Journal of Hydrologic Engineering*, 19(6), pp. 1160–1172. doi: 10.1061/(asce)he.1943-5584.0000878.

Supplementary Files

This is a list of supplementary files associated with this preprint. Click to download.

- Supplementarysection.docx